A Strand Entangled Supramolecular PANI/PAA Hydrogel enabled Ultra-stretchable Strain Sensor

Dong Liu[§], Honghao Zhou[§], Yuanyuan Zhao, Chenxi Huyan, Zibi Wang, Hamdi Torun, Zhanhu Guo, Sheng Dai[*], Ben Bin Xu[*] and Fei Chen[*]

D. Liu, Y. Zhao, C. Huyan, Z. Wang, and F. Chen

School of Chemical Engineering and Technology, Xi'an Jiaotong University, Xi'an, 710049, P.R. China.

E-mail: feichen@xjtu.edu.cn

H. Zhou, H. Torun, Z. Guo and B. B. Xu

Mechanical and Construction Engineering, Faculty of Engineering and Environment, Northumbria University, Newcastle upon Tyne, NE1 8ST, UK.

E-mail: ben.xu@northumbria.ac.uk

Y. Zhao

The 41st Institute of the Forth Academy, China Aerospace Science and Technology Corporation, Xi'an, Shaanxi, 710025, P.R. China.

S. Dai

School of Chemical and Process Engineering, University of Leeds, Leeds, LS2 9JT,UK

§: Equal contribution

Keywords: strain sensor, ultra-stretchable, hydrogel, doping effect, entanglement

Abstract

Hydrogel electronics have attracted growing interests for the emerging applications in personal healthcare management, human-machine interaction, etc. Herein, we propose a novel 'doping then gelling' strategy to synthesize supramolecular PANI/PAA hydrogel with a specific strand entangled network, by doping the PANI with acrylic acid (AA) monomers to avoid the PANI aggregation. The high-density electrostatic interaction between PAA and PANI chains serve as dynamic bond to initiate the strand entanglement, enabling PAA/PANI hydrogel with ultra-stretchability (2830%), high breaking strength (120 kPa), and rapid self-healing properties. Moreover, we develop the PAA/PANI hydrogel based sensor with a high strain sensitivity (gauge factor = 12.63), a rapid responding time (222 ms), and a robust conductivity based sensing behavior under cyclic stretching. We also demonstrate a set of strain sensing applications to precisely monitor human movements, indicating a promising application prospect as wearable devices.

1. Introduction

Flexible sensor that can rapidly and efficiently translate external stimulus into electrical signals without disturbing human activities, have been recognised as an essential component in the future wearable electronics for human health monitoring[1-4]. The sensing material plays a key role for developing high-performance flexible sensor, which are expected to have excellent mechanical strength, wide operation range, favorable antifatigue property, and good biocompatibility[5-8]. Hydrogels with three-dimensional crosslinked porous microstructures have emerged as one of the most promising candidates[9, 10], due to their similarities to natural tissues, excellent flexibility, bio-compatibility and self-healing ability[11-13].

Electrically conductive hydrogel (ECH) has been regarded as a feasible alternative to inorganic material to develop wearable sensor with a number of advantages [14, 15]. ECH is usually based on hydrophilic polymers such as polyvinyl alcohol (PVA), polyacrylamide (PAM), or polyacrylic acid (PAA) with intrinsic tunable mechanical property and excellent biocompatibility[16]. Among various conductive fillers, CPs (such as polyaniline (PANI), polypyrrole (PPy), and poly(3,4-ethylene-dioxythiophene) (PEDOT)) with specific π-conjugated systems possess high electrical conductivity, desirable mechanical properties, easy processibility, and extraordinary biocompatibility, placing them as an optimal choice to construct ECHs[17-19]. The unique organic and polymeric structure of CPs possesses diverse chemical modification sites to be integrated with the hydrophilic hydrogel network to pave uniformly dispersed conductive pathway[20, 21]. The constructed ECHs based wearable sensors exhibited a superior workable strain sensing range, low strain recognition limit, high electrical conductivity, and favorable strain sensitivity.[22-24]

Despite the potential merits of sensing properties for ECHs, an ideal wearable strain sensor needs to be mechanical comparability with human tissue, allow them to

work for different purposes. The CPs based doping method can unlock new features to modulate morphology and physical/chemical properties by introducing crosslinking, steric effects, and self-assemble capbility[25, 26] with multi-functional crosslinkers such as phytic acid, carbon dots, or borax[27-29]. However, the chain of conductive polymer, normally rigid and hydrophobic, may cause structural inhomogeneity and aggregation, leading to the destruction of path for electron transportation and thus the under performance of sensor[30, 31]. The doping interactions initialized by chemical cross-linkers brings conservative energy dissipation, thus resulting into low elongation for ECHs under deformation.

In this work, we proposed a novel 'doping then gelling' strategy to construct an ultra-stretchable supramolecular PAA/PANI hydrogel with entangled network. PANI was firstly doped with acrylic acid (AA) monomer, which not only allowed PANI to dissolve in water but also to enhance the conductivity of PANI. Secondly, we synthesize PAA/PANI hydrogels with high density electrostatic interactions as dynamic bonds, to realise PAA/PANI hydrogel with ultra-stretchability (2830%), high breaking strength (120 KPa) and rapid self-healing capabilities. Also, the resultant ECH exhibits excellent sensing ability attributed by the homogeneous conductive network.

2. Results and discussion

The 'doping then gelling' strategy is based on a stepwise approach (Figure 1a and Figure S1) to fabricate ultra-stretchable PAA/PANI hydrogel. The rod-shaped PANI was firstly synthesized, where the obtained nanoparticles easily aggregated (Figure S2) to make the solution opaque, owing to the π-π interaction between the polymer chains and the natural hydrophobicity of PANI. The subsequent addition of AA into the above PANI solution (denoted as AA/PANI) gradually made the mixture transparent. The AA with carboxyl group serves as a counterion to dopant protonates the imine groups in

PANI, while the carbonyl group enhances the solubility of PANI, resulting in uniform polymer chain dispersion. [32] This enhancement of solubility of PANI enabled by the doping interaction was also verified by digital photo and TEM images in Figure S3.

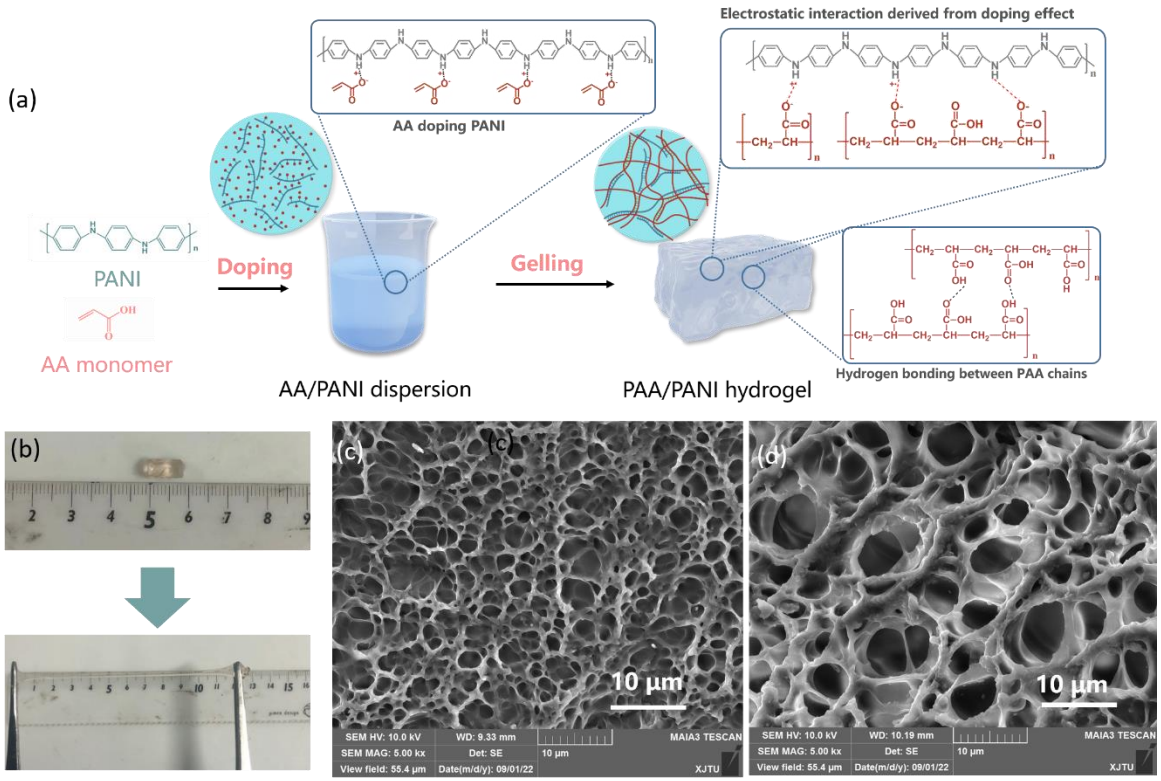

Figure 1. (a) Schematic illustration of synthesis process for PAA/PANI hydrogel; (b) The demonstration of excellent stretchability; SEM image of PAA/PANI-3 hydrogel (c) and PAA hydrogel (d).

The size distribution of AA/PANI is around 500 nm (Figure 2a), which is smaller than the average size of PANI in DI water (700 nm). When the polymerization of PAA completed, the abundant carboxyl group on PAA initiates electrostatic interactions with PANI molecular chains, where the cation radicals ($-NH^{3+}$) generated from the oxidation of aniline monomers are integrated with the PAA network that contains anion radicals ($-COO^{-}$) *via* strong electrostatic interactions and intermolecular hydrogen bonds. These strong intermolecular dynamic interactions reinforce the microstructure by offering a tough porous network in hydrogel (Figure 1c and 1d), and PAA/PANI-3 hydrogels possess smaller and denser micropores than that of the PAA hydrogel, demonstrating a strong strand entanglement between PAA and PANI chains,

resulting into excellent mechanical properties.

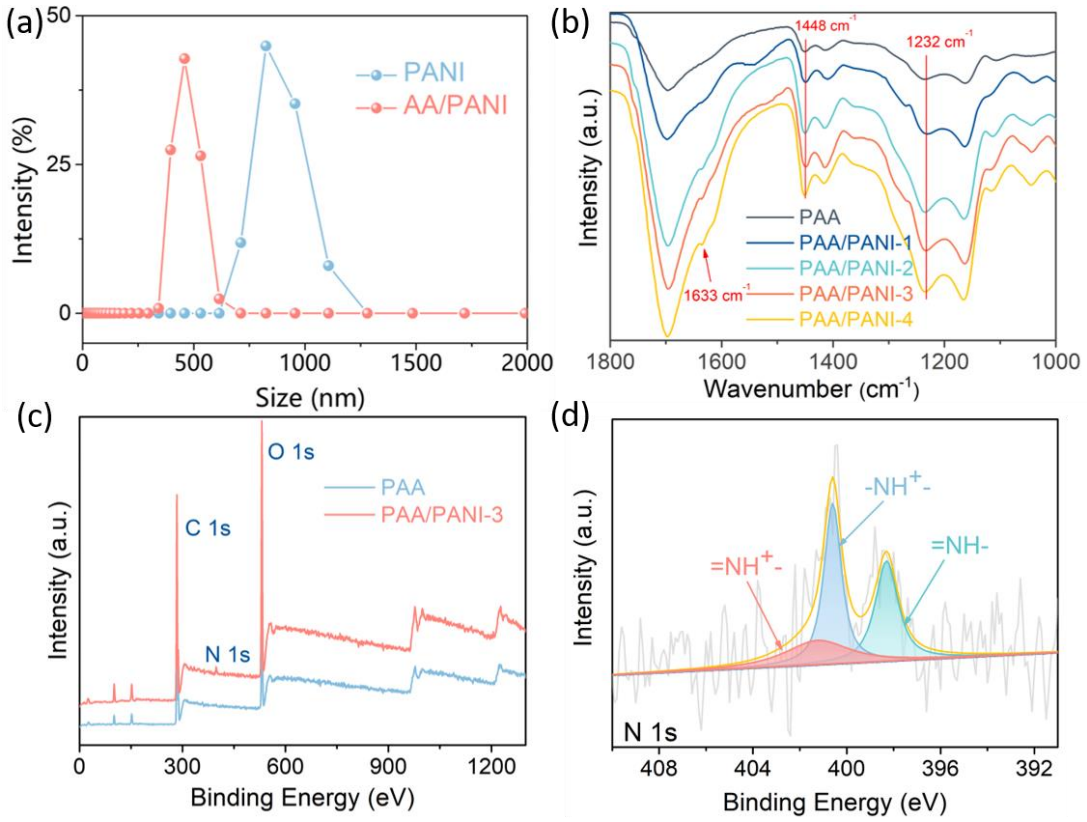

Figure 2. (a) Particle size distribution of PANI in water and AA aqueous solution; (b) FT-IR spectra of PAA and PAA/PANI hydrogels; (c) XPS spectra of PAA and PAA/PANI-3 hydrogels; (d) XPS high-resolution spectrum of N1s for PAA/PANI-3.

The prepared PAA/PANI hydrogel demonstrates exceptional tensile elasticity, as it is mechanically robust and can be stretched for tens of its initial length (Figure 1b, Movie S1). The PAA/PANI hydrogels exhibit relatively lower equilibrium swelling ratio than that of the PAA hydrogel, revealing the entangled supramolecular structure of PAA/PANI hydrogel (Figure S4). When swelling for 20 h, all the PAA/PANI hydrogels reach the dynamic equilibrium, notably shorter than that of PAA hydrogel. This phenomenon is attributed to that the entangled molecular chains of PAA/PANI hydrogels will slip, and disentangle during the initial swelling process. But continuing to soak in water, the disentangle process reach dynamic equilibrium and the swelling ratio keep constant due to the limit of dense microporous structures endowed by entangled molecular chains and dynamic interactions. While for the PAA hydrogel, the

connected microporous structure is only supported by dynamic interactions between PAA chains, which provides more space for the interring of external water during swelling process.

We performed the Fourier transform infrared spectrometry (FT-IR, Figure 2b and Figure S5) to identify the interactions between PAA and PANI chains. It is found that PANI has been successfully cooperated to PAA and the as-prepared PAA/PANI hydrogels are mixed at the molecular level[33, 34] (detailed in *Supplemental Information*). The X-ray photoelectron spectroscopy (XPS) result in Figure 2c, especially the N 1s in PAA/PANI-3 reveals the successful integration of PANI to PAA. The N 1s peak can be divided into three peaks (Figure 2d) with their binding energies of 398.3 eV, 400.6 eV and 401.2 eV, which correspond to the quinoid imine/benzenoid amine (=N–/–NH–) typed nitrogen (<400 eV), and positively charged nitrogen (-NH^+– and =NH^+–) species, respectively[35-38]. The doping level of PANI in the PAA/PANI hydrogel can be further calculated by the intensity ratio of charged nitrogen (-NH^+– and =NH^+–) to the total nitrogen content (N total). The specific doping values of PAA/PANI-1, PAA/PANI-2, PAA/PANI-3 and PAA/PANI-4 are calculated to be 60.6%, 65.6%, 58.3% and 61.2%, respectively, corresponding to the high density of chemical interactions to fulfil the strand entanglement between PAA and PANI.

We next investigate the mechanical property of PAA/PANI hydrogel. The tensile strength, elongation at break and toughness for all PAA/PANI hydrogels are higher than those of pure PAA hydrogel (Figure 3a), attributing to the strong electrostatic interactions that are derived from the doping effect between PAA and PANI. Furthermore, PAA/PANI-2 exhibit the highest ultimate strain of 2830% at a strength of about 120 kPa, while PAA/PANI-3 possess highest toughness of 1.542 MJ m^{-3} (Figure 3b). When introducing PANI into PAA, low content of PANI chains can be dispersed uniformly with generating the electrostatic bonds between PAA and PANI to

significantly enhance the mechanical properties (tensile strength, elongation, and fracture toughness) (Figure S6). The doping effect yield a strand entanglement with energy dissipation sites to enable the ultra-stretchability with the following reasons: (1) There are no aggregation among the π-π stacking between benzenoid rings in PANI chains, because the AA could facilitate the PANI chains to highly dispersed in water, resulting in a highly homogeneous hydrogel with no stress concentration area upon external forces. (2) When the hydrogel is stretched, the dynamic electrostatic bonds between PANI and PAA in the hydrogel could be slipped or fractured to dissipate energy upon a mechanical deformation to prevent the propagation of cracks[39-41]. However, the mechanical properties of PAA/PANI hydrogel degrade sharply when adding PANI more than 3 mg, due to the aggregation of PANI. To gain a clear understanding of the network structure during strain, a schematic representation is proposed in Figure 3c. On the one hand, it is projected that the dynamic noncovalent bonds between PAA and PANI chains are predicted to be readily fractured and act as reversible "sacrificial bonds" to help with energy dissipation during the deformation process. On the other hand, the tangled network is partially disentangled to dissipate the applied energy and transform the stress to avoid the fracture of polymer chains, resulting in high toughness and excellent self-recovery behavior of the PAA/PANI hydrogels. Compare to the recently reported conductive hydrogels prepared by crosslinking between CPs and hydrophilic polymer matrix, PAA/PANI hydrogel in this work possessed highest elongation and relatively lower toughness, thus broadening the application of ECHs for different purposes (Table 1).

Table 1. A rough comparison of the mechanical performance between this work and previously reported conductive hydrogels.

Hydrogel	Elongation	Tensile strength	Toughness	Ref.

		(MPa)	(MJ m^{-3})	
PAA/PANI	1160%	0.30	0.267	[22]
PANI/CS-PAAm	927%	2.62	8.67	[24]
PANI-PAAm-GOCS	360%	0.8	3.91	[42]
PVA/PA/PANI/GA CCH	670%	1.2	2.5	[43]
PAA/PPy-Fe	448%	0.57	-	[44]
PANI/P(AAm-*co*-HEMA)	530%	7.27	9.19	[45]
PAA/PANI	2830%	0.12	1.54	This work

The formation of dynamic bond is instant and automatic, with little delay for carboxyl group to graft onto the charged nitrogen in PANI chains. As shown in Figure 3d, small hysteresis has been observed on the tensile stress-strain curve for the PAA/PANI-3 hydrogel. The ratios of dissipated energy to applied work that displayed in Figure 3e are only about 10% under various strain, revealing an elastic behaviour for PAA/PANI-3 hydrogel[46]. The stress-strain results in Figure S7 also suggest the mechanical performance of PAA/PANI-3 are independent to the stretch rate, with a small deviation caused by the strand entangled structure [47]. Together with a good elasticity, the results indicate that the dense hydrogen bonds between PANI and PAA can be dissociate-reassociate rapidly, which is favourable to use PAA/PANI-3 hydrogel for cyclic sensing.

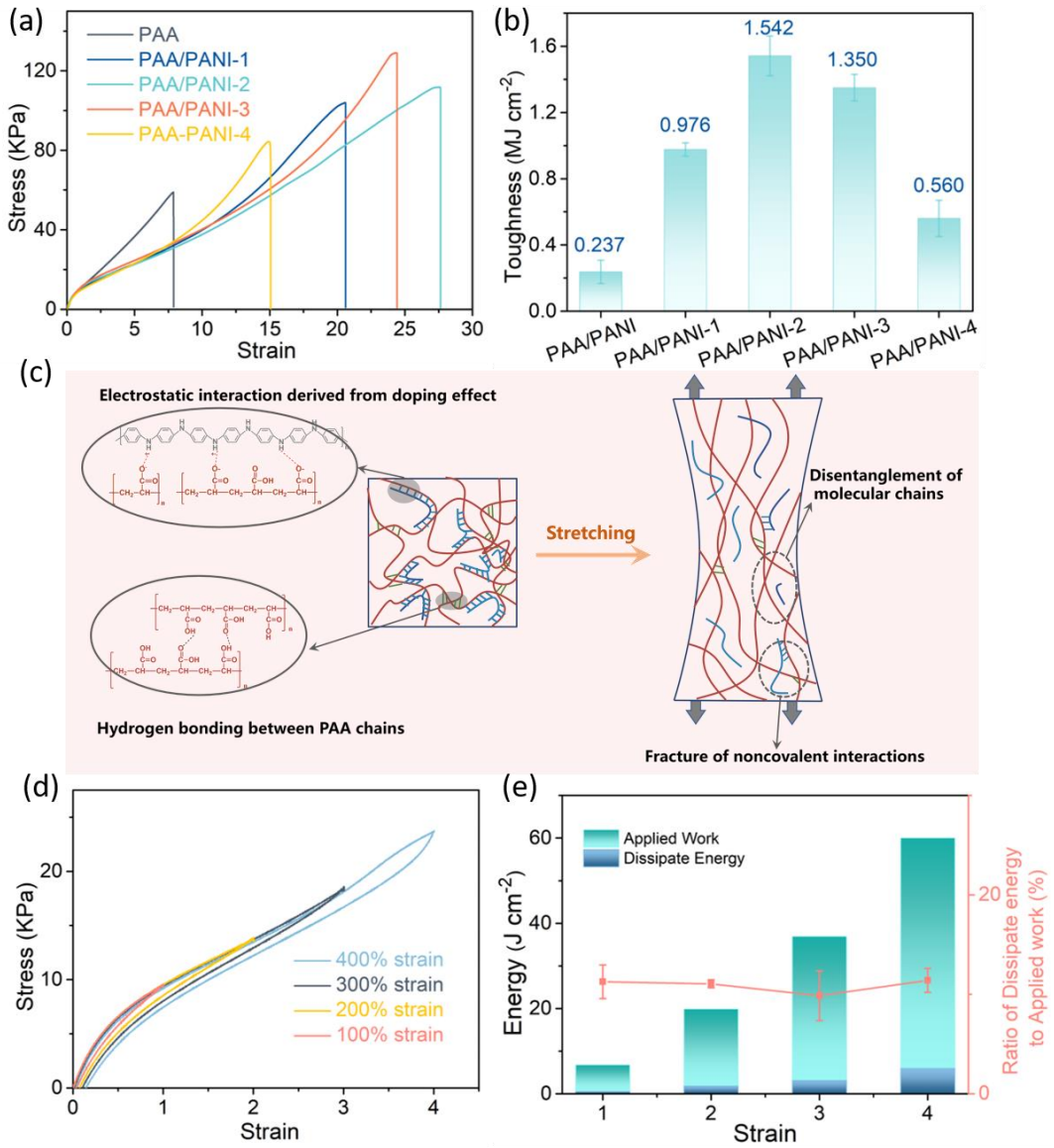

Figure 3. (a) Tensile stress–strain curves, and (b) toughness of PAA and PAA/PANI hydrogels; (c) Schematic illustration of the strain mechanism of PAA/PANI hydrogel; (d) Hysteresis curves of PAA/PANI-3 hydrogel during loading and unloading cycles (100, 200, 300 and 400%); (e) the applied work and dissipated energy of PAA/PANI-3 hydrogel during loading and unloading cycles.

To further study the dynamic interaction between PANI and PAA, we assess the self-healing ability of PAA/PANI-3 hydrogel. As shown in Figure 4a, we cut a PAA/PANI-3 hydrogel cylinder into two parts, and then brought them into full contact with each other. After ten seconds, two separated parts join into a single piece as the result of a self-healing process, with the integrity of structure well maintained under bending. The tensile stress-strain curves of the original and self-healed PAA/PANI-3

hydrogels are presented in Figure 4b, unveiling that the PAA/PANI-3 hydrogel recover to about 86.2% of original mechanical strength after self-healing for 24 h at 25 °C. The self-healing is driven by the reversible hydrogen bond between PAA chains and dynamic electrostatic bonds between PANI and PAA chains[48]. After attaching two parts, the hydrophilic segments in the PAA chains re-associate to generate new hydrogen bonds. Simultaneously, the dynamic interfacial interactions among the free positive charged nitrogen species (-NH^+– and =NH^+–), –OH, and –COO- groups occur and reform the entangled network, leading to the self-healing. Inspired by the favourable mechanical performance after self-healing, we monitored the electrical property variations of PAA/PANI-3 hydrogel during fracture/self-healing. As Figure 4c shows, when a PAA/PANI-3 hydrogel was completely cut off, the resistance dramatically increased from the stable state to the open circuit state. Once two fractured pieces were brought together, the resistance quickly returned to the original value within 11.6 s in several cutting-healing cycles, which also revealed the intriguing self-healing property.

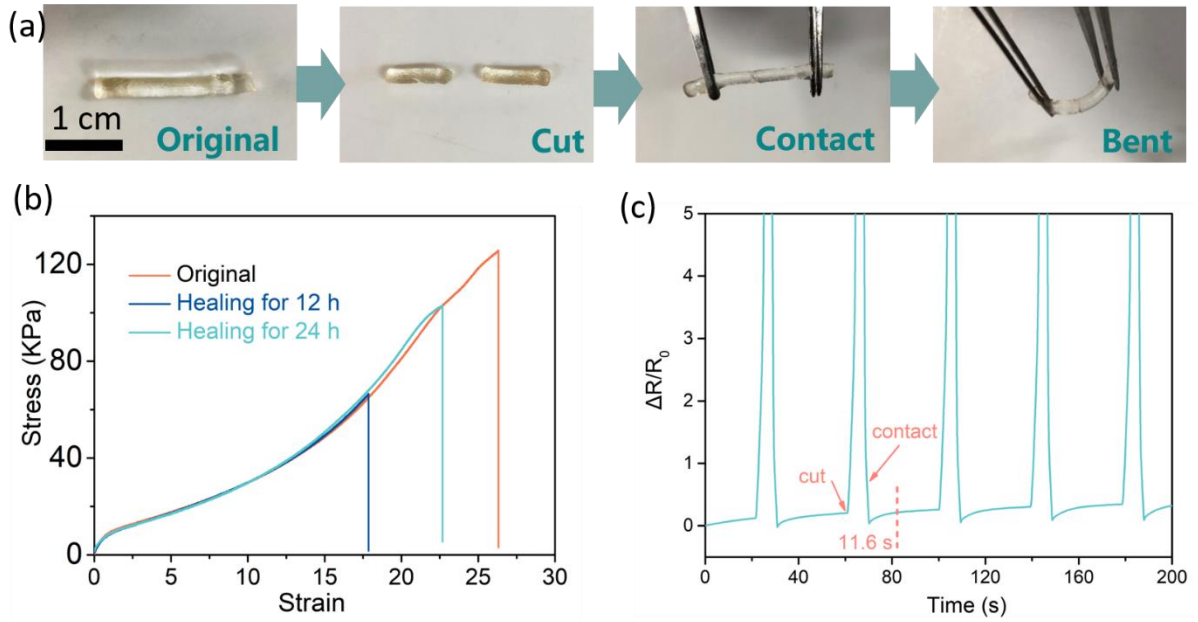

Figure 4. (a) Optical images showing the self-healing behaviour of PAA/PANI-3 hydrogel; (b) Tensile stress–strain curves of the healed PAA/PANI-3 hydrogel with the

indicated healing time; (c) conductively self-healing ability of the PAA/PANI-3 hydrogel.

We also investigate the electromechanical property of PAA/PANI-3 hydrogel under stretching, with the set-up sketched in Figure 5a. We focus on understanding the relationship between strain and $\Delta R/R_0$ ($\Delta R=R-R_0$, R_0 and R refer to the resistances of the original and loaded hydrogels, respectively). As shown in Figure S8, stable and reversible $\Delta R/R_0$ data can be obtained while the sensor was stretched in a cycle of introducing strain levels of 20%, 40%, 60% and 100% strain. Gauge factor (GF), $GF=(\Delta R/R_0)/\varepsilon$, is a commonly used parameter to assess the sensitivity. For the PAA/PANI-3 hydrogel sensor (Figure 5b), the GF value is 3.21 at low strain from 0 to 200%, and increased to 6.11 at higher strain from 200% to 800%, then up to 12.63 under highest strain range of 800%-2000%, comparable to that of recently reported hydrogel sensors[49-52]. Figure 5c illustrates the change in resistance for the PAA/PANI-3 hydrogel sensor with various cyclic strains under a speed of 100 mm/min. It is noteworthy to mention that the sensor can work in a wide range from 1% to 400%, with outstanding reproducibility and reliability. In Figure 5d, the electrical signals clearly reflect a frequency-dependent feature when the hydrogel sensor is tested under different stretching frequencies (0.04–0.32 Hz).

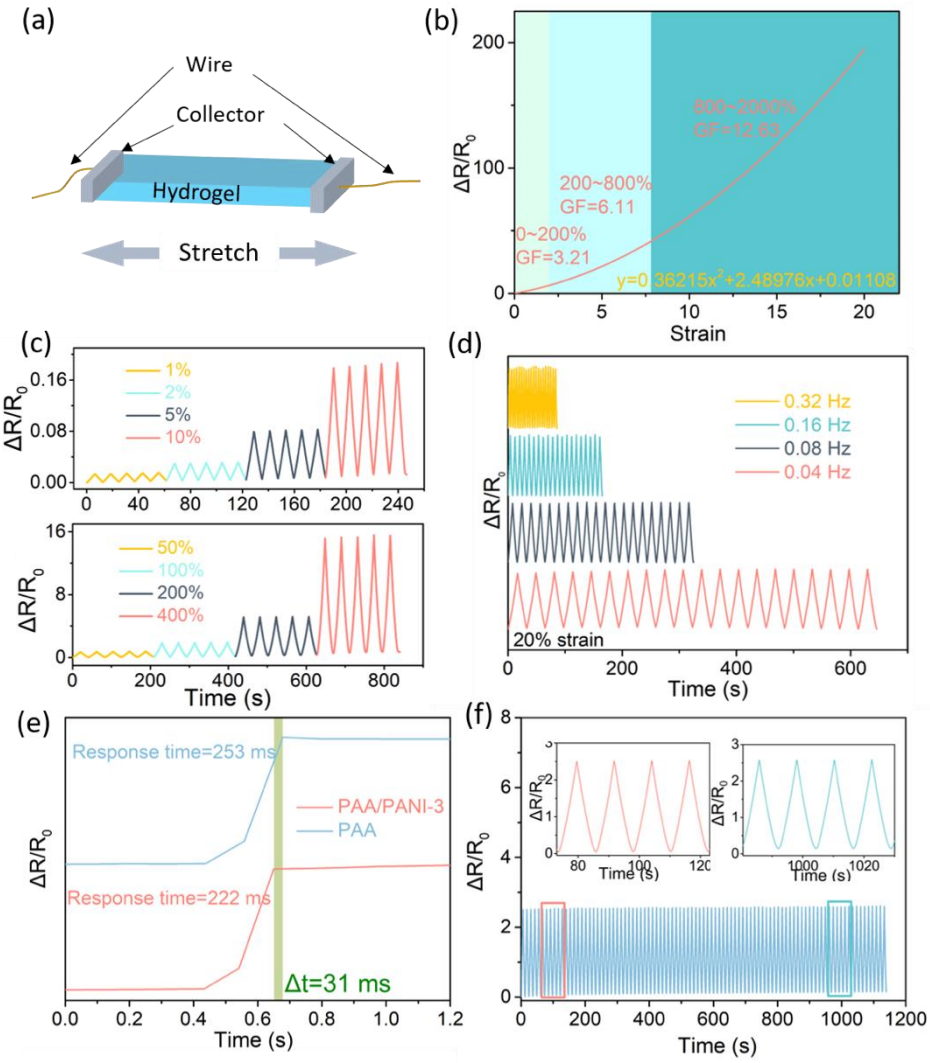

Figure 5. (a) Schematic illustration of the hydrogel-based sensor; (b) $\Delta R/R_0$ versus applied strain from 0 to 2000% of the PAA/PANI-3 hydrogel sensor; (c) $\Delta R/R_0$ of the hydrogel senor in response to tiny strain and large strain; (d) The hydrogel senor generated response to frequency from 0.04 Hz to 0.32 Hz; (e) Response times of the PAA and PAA/PANI-3 hydrogel sensors; (f)100 continuous 100% stretching cycles of PAA/PANI-3 hydrogel sensor.

This favourable electromechanical property of PAA/PANI hydrogel is mainly resulted from the dynamic entangled network. When deforming hydrogel sensor, the homogeneity of conductive network is disrupted, lead to the change of conductivity. When the hydrogel is reinstated, the resistance can be recovered to the original state owing to the restoration of conductive network.[53] Moreover, PANI efficiently increases the electrical conductivity of hydrogel due to the doping effect of PAA

molecules to PANI.[54] The measured conductivity (σ) of PAA/PANI-3 is 1.18 mS cm^{-1}, which is an order of magnitude higher than that of the PAA hydrogel (0.137 mS cm^{-1}), leading to faster electron transfer speed (Figure S9). We also evaluate the responding time for PAA/PANI-3 and PAA hydrogels (Figure 5e) at 1% strain. The results suggest that the PAA/PANI-3 hydrogel has a faster response time of 222 ms, compared to that of PAA hydrogel (253 ms). The robustness of the electromechanical sensing performance is also examined by cyclic test (Figure 5f). The hydrogel possesses stable and reproducible response signals after 100 continuous 100% tensing loading-unloading cycles, and the small shift of baseline mainly due to the hysteresis during shape recovery[55]. The inset in Figure 5f shows the relative resistance values measured from 7 to 10 cycles and 85–88 cycles, where both the maximum and minimum values remain constant, revealing the good stability of the sensor. Similarly, the PAA/PANI-3 hydrogel after self-healing showed excellent signal stability (Figure S10), showing the potential of the sensor application.

We next demonstrate the application of using the PAA/PANI-3 hydrogel-based sensor to detect human motions in different scenarios. In Figure 6a, the pronunciation of different words, such as “nihao” and “xjtu” can be recognized when attaching the hydrogel sensor to neck of volunteer, a reproducible resistance changes with specific peak waveforms presenting for different words. The frequency response of the sensor allows differentiating distinct sounds during speech. In Figure 6b, a sensor is deployed on volunteer’s cheek to sense the subtle physiological changes on face in a conformal fashion. Interestingly, the sensor detects the localized epidermal deformation every time when volunteer smiles, with a signature signal produced to record the event. Based on the high sensitivity and the frequency-dependency, the PAA/PANI-3 hydrogel can sense the vibrations. Motivated by the exceptional sensing feature of the PAA/PANI-3 hydrogel under micro strain (0.1–0.5% strain), we also presented the

radial artery pulse beating detection data with profiles of $\Delta R/R_0$ as a function of time. The plotted curves, as seen in Figure 6c, exhibit good regularity and reproducibility, while the heart rate can be counted to be 71 bpm. In addition to the effectively sensing the subtle physiological changes, our strain sensor can precisely detect deformation when it is placed on knee joints to detect the motions (Figure 6d) such as standing, squatting, walking and running with specific output signals. Same principle also allows the sensor to monitor the bending of a finger joint (Figure 6e, Movie S2) under cyclic bending condition. The excellent capacity to detect human activity has led to the development of PAA/PANI-3 hydrogel, which allows for easier and more accurate strain detection as well as physiological signal monitoring.

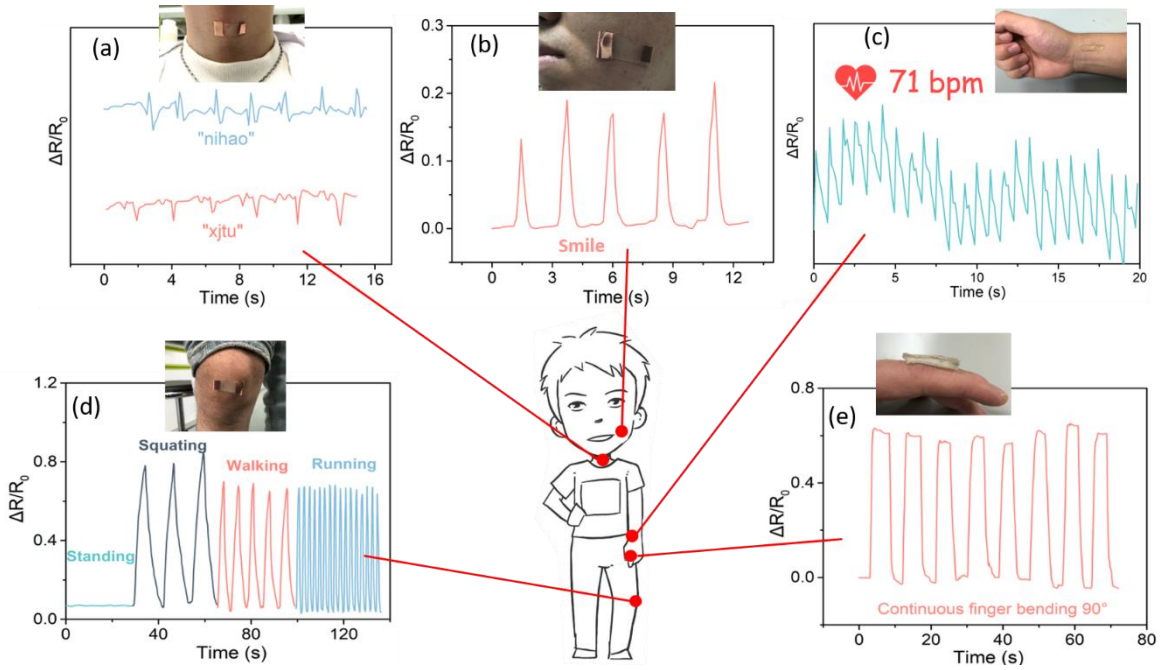

Figure 6. The real-time sensing performance of PAA/PANI-3 gel sensor, with the corresponding signals from (a) throat vocalization, (b)cheek, (c) wrist, (d) knee and (e) finger.

Finally, we develop a 2D tactical sensor comprises a 3 × 3 array of PAA/PANI-3 hydrogels, copper wires, and a PET film to detect the distribution of forces, as shown in Figure S11. Each conductive hydrogel cube acted as a sensing unit/pixel (Figure 7a inset). In a demonstration experiment, the responses of individual units are shown in

Figure 7 when a finger was placed on the units labelled as B2 and B1. The responses of the units were recorded simultaneously and were displayed on a computer (Figure 7b and 7d). It is feasible to extend this method to realise integrated sensing arrays in large formats for applications as touchpads and E-skins, as recently reported. [56]

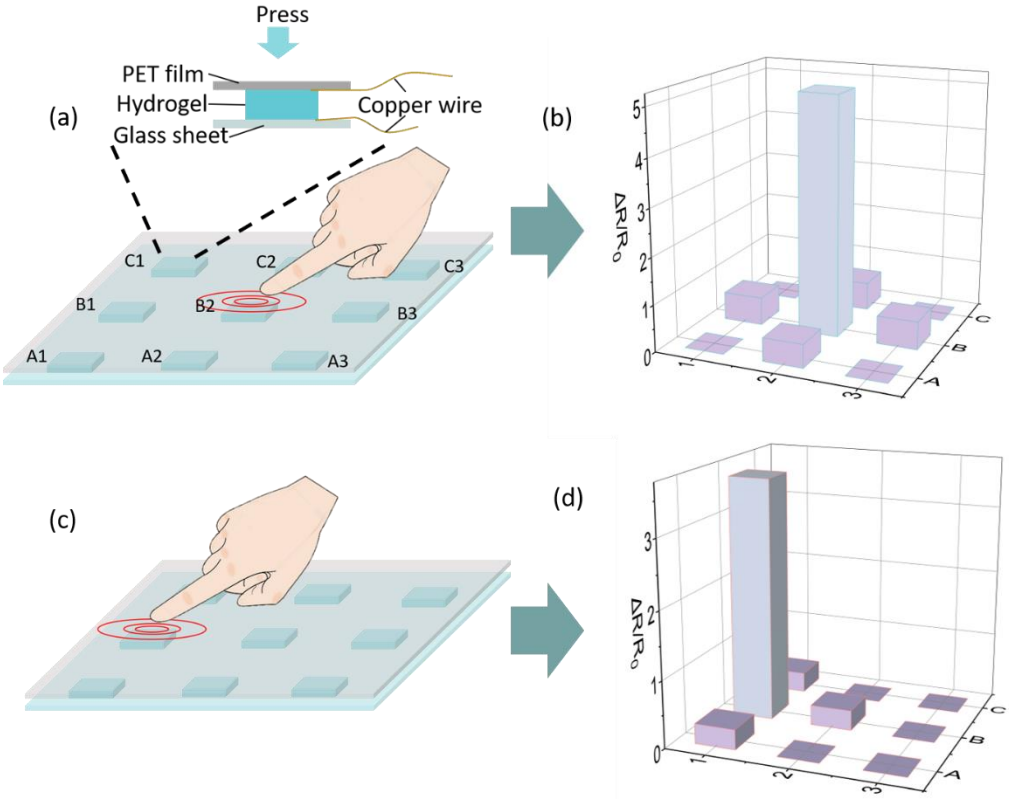

Figure 7. The 3 × 3 array of strain sensors that PAA/PANI-3 hydrogel cubes: Press the B2 (a, b) and B1 (c, d) pixels in the array.

3. Conclusion

In summary, we described a 'doping then gelling' strategy to achieve ultra-stretchable PAA/PANI hydrogel by constructing a conductive PAA/PANI strand entangled network. The electrostatic bonds between PANI and PAA act as dynamic bonds to initiate the strand entangled network, providing PAA/PANI hydrogel with superior mechanical performances such as ultra-high stretchability, toughness, and favourable self-healing capability. In addition, the introduction of PANI fulfil the hydrogel with improved sensitivity and a faster responding time. Benefiting from above mechanical and mechanical-electrical features, the assembled PAA/PANI hydrogel based sensor

present robust sensing performance to monitor human motions at both small deformations (the tiny physiological motions, i.e. speaking and mouth opening) and large motions (squatting, walking and joggering). The PAA/PANI hydrogel also has potential to be used as 2D tactical board for human-machine interface and/or E-skin.

4. Experimental Section

Materials and Reagents

AA (AR, 99%), potassium persulfate (KPS) (99.5%), ammonium persulfate (APS, AR) and ethanol (AR) were purchased from Shanghai Macklin Biochemical co., Ltd (Shanghai, China). Methylene-bis-acrylamide (MBAA) (99%) was supplied by Sinopharm Chemical Reagent Co., Ltd (Shanghai, China). Aniline monomer (99%) was obtained from Shanghai Adamas Regent, Co., Ltd. AA was distilled to remove the polymerization inhibitor prior to use. Deionized (DI) water was generated from a Millipore system.

Preparation of PAA/PANI hydrogel

PANI was first prepared via the *in situ* chemical oxidative polymerization of aniline. 5.0 mL APS aqueous solution (molar ratio to aniline of 1:1) was dropped into aniline solution and maintained at room temperature for 6 h. PANI was collected after filtration and washing. After that, known amount of dry PANI was re-dispersed into 25 mL 7.5 M AA aqueous solution. The obtained homogenous solution was mixed with 0.12 mM KPS and 0.27 mM MBAA and bubbled nitrogen for 20 min. Finally, the mixture was injected into a reaction mould and cured at 50 ^{o}C for 4 h to obtain the PAA/PANI hydrogel. The nomenclature of PAA/PANI-X denoted production with varying amount of PANI (X was PANI feeding mass), for example, PAA/PANI-1 denoted adding 1 mg PANI during the synthesis.

Characterization

The morphology of PANI and PANI-AA was characterized by a TEM (JEOL JEM-2100Plus, Japan), while an SEM (MAIA3 LMH, from TESCAN, USA) was used to investigate the surface of freeze-dried PAA/PANI hydrogels. DLS (Zetasizer Nano ZSE, from Malvern, UK) were used to examine the diameter of the PANI in water and the AA aqueous solution. The chemical structures of PAA/PANI hydrogels were studied by the Nicolet iS50 FTIR spectrometer (Shanxi, China) in the spectral range of 650-4000 cm^{-1}. The mechanical tensile tests were conducted by the CMT1503 universal mechanical tester (SUST, Zhuhai, China) equipped with a 200 N tension sensor. All human sensing demonstrations were performed in Xi'an Jiaotong University (China), where the project was fully assessed and approved by the university ethic committee with the consent issued from the participant.

Supporting Information

Supporting Information is available from the Wiley Online Library or from the author.

Acknowledgements

This work was supported partially by the China Postdoctoral Science Foundation (2020M683469), the National Natural Science Foundation of China (No. 21803040) , Young Talent Support Plan of Xi'an Jiaotong University and the Engineering and Physical Sciences Research Council (EPSRC, UK) grant-EP/N007921.

Received: ((will be filled in by the editorial staff))
Revised: ((will be filled in by the editorial staff))
Published online: ((will be filled in by the editorial staff))

References

[1] Peng, Q.; Chen, J.; Wang, T.; Peng, X.; Liu, J.; Wang, X.; Wang, J.; Zeng, H., *InfoMat* **2020,** *2* (5), 843-865.

[2] Wang, Z.; Zhou, H.; Liu, D.; Chen, X.; Wang, D.; Dai, S.; Chen, F.; Xu, B.B., *Adv. Funct. Mater.* **2022,** *32*(25), 2201396.

[3] Song, L.; Chen, J.; Xu, B.B.; Huang, Y., *ACS Nano* **2021,** *15* (12), 18822-18847.

[4] Zhang, W.; Wu, B.; Sun, S.; Wu, P., *Nat. Commun.* **2021,** *12* (1), 4082.

[5] Zhang, Z.; Gao, Z.; Wang, Y.; Guo, L.; Yin, C.; Zhang, X.; Hao, J.; Zhang, G.; Chen, L., Eco-Friendly, *Macromolecules* **2019,** *52* (6), 2531-2541.

[6] Wei, H.; Wang, Z.; Zhang, H.; Huang, Y.; Wang, Z.; Zhou, Y.; Xu, B.B.; Halila, S.; Chen, J., *Chem. Mater.* **2021,** *33*(17), 6731-6742.

[7] Liu, X.; Wu, J.; Qiao, K.; Liu, G.; Wang, Z.; Lu, T.; Suo, Z.; Hu, J., *Nat. Commun.* **2022,** *13* (1), 1622.

[8] Lei, Z.; Huang, J.; Wu, P., *Adv. Funct. Mater.* **2019,** *30*(19), 1908018.

[9] Liang, X.; Chen, G.; Lin, S.; Zhang, J.; Wang, L.; Zhang, P.; Lan, Y.; Liu, J., *Adv. Mater.* **2022,** *34* (8), e2107106.

[10] Zhang, K.; Chen, X.; Xue, Y.; Lin, J.; Liang, X.; Zhang, J.; Zhang, J.; Chen, G.; Cai, C.; Liu, J., *Adv. Funct. Mater.* **2021,** *32*(15), 2111465.

[11] Pan, L.; Yu, G.; Zhai, D.; Lee, H.R.; Zhao, W.; Liu, N.; Wang, H.; Tee, B.C.; Shi, Y.; Cui, Y.; Bao, Z., *Proc. Natl. Acad. Sci. U.S.A.* **2012,** *109* (24), 9287-9292.

[12] Lei, Z.; Zhu, W.; Zhang, X.; Wang, X.; Wu, P., *Adv. Funct. Mater.* **2020,** *31* (8), 2008020.

[13] Zhang, Y.; Liu, K.; Liu, T.; Ni, C.; Chen, D.; Guo, J.; Liu, C.; Zhou, J.; Jia, Z.; Zhao, Q.; Pan, P.; Xie, T., *Nat. Commun.* **2021,** *12* (1), 6155.

[14] Yang, J.C.; Mun, J.; Kwon, S.Y.; Park, S.; Bao, Z.; Park, S., *Adv. Mater.* **2019,** *31* (48), e1904765.

[15] Chortos, A.; Liu, J.; Bao, Z., *Nat. Mater.* **2016,** *15* (9), 937-950.

[16] Feng, Y.; Liu, H.; Zhu, W.; Guan, L.; Yang, X.; Zvyagin, A.V.; Zhao, Y.; Shen, C.; Yang, B.; Lin, Q., *Adv. Funct. Mater.* **2021,** *31*(46), 2105264.

[17] Xia, Y.; Zhu, H., *Soft Matter* **2011,** *7* (19), 9388.

[18] Yang, T.; Xu, C.; Liu, C.; Ye, Y.; Sun, Z.; Wang, B.; Luo, Z., *Chem. Eng. J.* **2022,** *429*, 132430.

[19] Ren, K.; Cheng, Y.; Huang, C.; Chen, R.; Wang, Z.; Wei, J., *J. Mater. Chem. B* **2019,** *7* (37), 5704-5712.

[20] Ge, G.; Lu, Y.; Qu, X.; Zhao, W.; Ren, Y.; Wang, W.; Wang, Q.; Huang, W.; Dong, X., *ACS Nano* **2020,** *14* (1), 218-228.

[21] Gan, D.; Shuai, T.; Wang, X.; Huang, Z.; Ren, F.; Fang, L.; Wang, K.; Xie, C.; Lu, X., *Nanomicro. Lett.* **2020,** *12* (1), 169.

[22] Wang, Z.; Zhou, H.; Lai, J.; Yan, B.; Liu, H.; Jin, X.; Ma, A.; Zhang, G.; Zhao, W.; Chen, W., *J. Mater. Chem. C* **2018,** *6* (34), 9200-9207.

[23] Hosseinzadeh, S.; Rezayat, S.M.; Vashegani-Farahani, E.; Mahmoudifard, M.; Zamanlui, S.; Soleimani, M., *Polymer* **2016,** *97*, 205-216.

[24] Cong, J.; Fan, Z.; Pan, S.; Tian, J.; Lian, W.; Li, S.; Wang, S.; Zheng, D.; Miao, C.; Ding, W.; Sun, T.; Luo, T., *ACS Appl. Mater. Interfaces* **2021,** *13* (29), 34942-34953.

[25] Huyan, C.; Ding, S.; Lyu, Z.; Engelhard, M.H.; Tian, Y.; Du, D.; Liu, D.; Lin, Y., *ACS Appl. Mater. Interfaces* **2021,** *13* (41), 48500-48507.

[26] Ma, Z.; Shi, W.; Yan, K.; Pan, L.; Yu, G., *Chem. Sci.* **2019,** *10* (25), 6232-6244.

[27] Wang, Z.; Zhou, H.; Chen, W.; Li, Q.; Yan, B.; Jin, X.; Ma, A.; Liu, H.; Zhao, W., *ACS Appl. Mater. Interfaces* **2018,** *10* (16), 14045-14054.

[28] Shit, A.; Heo, S.B.; In, I.; Park, S.Y., *ACS Appl. Mater. Interfaces* **2020,** *12* (30), 34105-34114.

[29] Ding, Q.; Xu, X.; Yue, Y.; Mei, C.; Huang, C.; Jiang, S.; Wu, Q.; Han, J., *ACS Appl. Mater. Interfaces* **2018,** *10* (33), 27987-28002.

[30] Liu, T.; Jiao, C.; Peng, X.; Chen, Y.N.; Chen, Y.; He, C.; Liu, R.; Wang, H., *J. Mater. Chem. B* **2018,** *6* (48), 8105-8114.

[31] Shi, Y.; Ma, C.; Peng, L.; Yu, G., *Adv. Funct. Mater.* **2015,** *25* (8), 1219-1225.

[32] Lu, X.; Ng, H.Y.; Xu, J.; He, C., *Synth. Met.* **2002,** *128* (2), 167-178.

[33] Wang, X.; Deng, J.; Duan, X.; Liu, D.; Guo, J.; Liu, P., *J. Mater. Chem. A* **2014,** *2* (31), 12323-12329.

[34] Tong, J.; Han, C.; Hao, X.; Qin, X.; Li, B., *ACS Appl. Mater. Interfaces* **2020,** *12* (35), 39630-39638.

[35] Hu, R.; Ji, G.; Wang, Y.; Zhao, J.; Zheng, J., *Extreme Mechanics Letters* **2021,** *42*, 101136.

[36] Feng, X.-M.; Li, R.-M.; Ma, Y.-W.; Chen, R.-F.; Shi, N.-E.; Fan, Q.-L.; Huang, W., *Adv. Funct. Mater.* **2011,** *21* (15), 2989-2996.

[37] Hao, Q.; Xia, X.; Lei, W.; Wang, W.; Qiu, J., *Carbon* **2015,** *81*, 552-563.

[38] Delcroix, M.F.; Huet, G.L.; Conard, T.; Demoustier-Champagne, S.; Du Prez, F.E.; Landoulsi, J.; Dupont-Gillain, C.C., *Biomacromolecules* **2013,** *14* (1), 215-225.

[39] Dai, X.; Du, Y.; Wang, Y.; Liu, Y.; Xu, N.; Li, Y.; Shan, D.; Xu, B.B.; Kong, J., *ACS Appl. Polym.* **2020,** *2* (3), 1065-1072.

[40] Miao, W.; Yang, B.; Jin, B.; Ni, C.; Feng, H.; Xue, Y.; Zheng, N.; Zhao, Q.; Shen, Y.; Xie, T., *Angew. Chem. Int. Ed. Engl.* **2022,** *61* (11), e202109941.

[41] Zheng, N.; Xu, Y.; Zhao, Q.; Xie, T., *Chem. Rev.* **2021,** *121* (3), 1716-1745.

[42] Jin, X.; Jiang, H.; Li, G.; Fu, B.; Bao, X.; Wang, Z.; Hu, Q., *Chem. Eng. J.* **2020,** *394*.

[43] Wei, H.; Kong, D.; Li, T.; Xue, Q.; Wang, S.; Cui, D.; Huang, Y.; Wang, L.; Hu, S.; Wan, T.; Yang, G., *ACS Sensors* **2021,** *6*(8), 2938-2951.

[44] Ginting, M.; Pasaribu, S.P.; Masmur, I.; Kaban, J.; Hestina, *RSC Adv.* **2020,** *10* (9), 5050-5057.

[45] Wang, Z.; Chen, J.; Cong, Y.; Zhang, H.; Xu, T.; Nie, L.; Fu, J., *Chem. Mater.* **2018,** *30* (21), 8062-8069.

[46] Kim, J.; Zhang, G.; Shi, M.; Suo, Z., *Science* **2021,** *374* (6564), 212-216.

[47] Zheng, D.; Lin, S.; Ni, J.; Zhao, X., *Extreme Mechanics Letters* **2022,** *51*, 101608.

[48] Wang, Z.; Liu, D.; Oleksandr, S.; Li, J.; Arumugam, S.K.; Chen, F., *Ind. Eng. Chem. Res.* **2021,** *60* (48), 17534-17544.

[49] Wang, Y.; Xia, Y.; Xiang, P.; Dai, Y.; Gao, Y.; Xu, H.; Yu, J.; Gao, G.; Chen, K., *Chem. Eng. J.* **2022,** *428*.

[50] Gao, Y.; Gu, S.; Jia, F.; Gao, G., *J. Mater. Chem. A* **2020,** *8* (45), 24175-24183.

[51] Wang, Y.; Gao, G.; Ren, X., *Polymer* **2021,** *215*, 123340.

[52] Li, X.; He, L.; Li, Y.; Chao, M.; Li, M.; Wan, P.; Zhang, L., *ACS Nano* **2021,** *15* (4), 7765-7773.

[53] Wu, J.; Han, S.; Yang, T.; Li, Z.; Wu, Z.; Gui, X.; Tao, K.; Miao, J.; Norford, L.K.; Liu, C.; Huo, F., *ACS Appl. Mater. Interfaces* **2018,** *10* (22), 19097-19105.

[54] Wang, T.; Zhang, Y.; Liu, Q.; Cheng, W.; Wang, X.; Pan, L.; Xu, B.; Xu, H., *Adv. Funct. Mater.* **2018,** *28* (7), 1705551.

[55] Yang, B.; Yuan, W., *ACS Appl. Mater. Interfaces* **2019,** *11* (18), 16765-16775.

[56] Wang, S.; Xu, J.; Wang, W.; Wang, G.N.; Rastak, R.; Molina-Lopez, F.; Chung, J.W.; Niu, S.; Feig, V.R.; Lopez, J.; Lei, T.; Kwon, S.K.; Kim, Y.; Foudeh, A.M.; Ehrlich, A.; Gasperini, A.; Yun, Y.; Murmann, B.; Tok, J.B.; Bao, Z., *Nature* **2018,** *555* (7694), 83-88.